MOLEKUL
eISSN: 2503-0310

Articles

https://doi.org/10.20884/1.jm.2022.17.1.5571

Tannic acid modified iron oxide nanoparticles and its application in protein adsorption: isotherm, kinetic, and thermodynamic study

Hans Kristianto*, Joshua Alexander, Susiana Prasetyo, Asaf K Sugih

Department of Chemical Engineering, Faculty of Industrial Technology, Parahyangan Catholic University, Ciumbuleuit 94, Bandung 40141, Indonesia

*Corresponding author email: hans.kristianto@unpar.ac.id

Received June 12, 2021; **Accepted** October 11, 2021; **Available online** March 20, 2022

ABSTRACT. Iron oxide nanoparticles, such as Fe_3O_4, are commonly used in various applications, such as drug delivery, magnetic fluid, water purification, and enzyme immobilization. These applications require protein to be adsorbed on the surface of iron oxide nanoparticles. However direct utilization of iron oxide nanoparticles has several drawbacks, thus modification of iron oxide nanoparticles is usually done. In this study, we reported surface modification of Fe_3O_4 using tannic acid to adsorb bovine serum albumin (BSA). The effect of modification and the BSA adsorption on the Fe_3O_4 was characterized using Fourier Transform Infrared Spectroscopy, X-ray Diffraction, Scanning Electron Microscopy, and Transmission Electron Microscopy. Furthermore the adsorption performance of modified and unmodified Fe_3O_4 was investigated at various initial pH, BSA concentration, and adsorption temperature. Several kinetic and isotherm adsorption models were used to describe the adsorption in this study. It was found that highest BSA adsorption was obtained at pH 4.8, near BSA's isoelectric point. The adsorption kinetics followed the pseudo 2nd order model and reached equilibrium after 210 min adsorption. Based on Langmuir monolayer adsorption capacity, it was found that tannic acid modified Fe_3O_4 had 5 times higher adsorption capacity (222 mg/g), compared to unmodified Fe_3O_4 (46 mg/g). Furthermore, from the thermodynamic study, it was suggested that the BSA adsorption was endothermic, spontaneous, and random in nature.

Keywords: adsorption; bovine serum albumin; iron oxide nanoparticles; tannic acid

INTRODUCTION

These days, study about nanomaterial size between 1 – 100 nm gained a lot of interest. This was possible due to a wide spectrum of possible applications. Among various nanomaterial, iron oxide nanoparticle was intensively studied as it has various advantages, such as low cost, low toxicity, highly magnetic, and high biocompatible (Laurent et al., 2008). However there are some drawbacks, such as high chemical activity and easily oxidized by air that could lead to lower magnetic property (Wu et al., 2008), and relatively unstable and tend to aggregate on account of its high energy surface (Xu et al., 2014). These drawbacks could lead to ineffective adsorption process.

It is known that stability of iron nanoparticles could be preserved by functionalization using multivalent acid. Several acids that have been used such as citric acid (Rahman et al., 2012), gallic acid (Dorniani et al., 2012), oxalic acid, succinic acid, and glutamic acid (Lesiak et al., 2019; Neha et al., 2017). One promising application of acid modified iron oxide nanoparticles is protein adsorption/immobilization. Adsorption of protein on iron oxide nanoparticles could be used for various application such as enzyme immobilization (Atacan et al., 2019), magnetic coagulant (Kristianto et al., 2020), drug delivery (Cagliani et al., 2019), protein purification (Cao et al., 2012), and adsorbent with enhanced adsorption capacity for wastewater treatment (Dalvand et al., 2016). Surface modification using organic acids, in the form of surface coat, is also known to assist protein adsorption, thus this method is commonly used for previously mentioned applications.

In this study, we investigated the effect of Fe_3O_4 modification using tannic acid to the protein adsorption performance. Tannic acid is a secondary polyphenolic compound that is commonly obtained from plants (Bele et al., 2010). Tannic acid has a high molecular weight decorated with hydroxyl functional groups. The presence of hydroxyls makes tannic acid water soluble and able to bind with protein (Cobellis et al., 2016). Tannic acid interactions with various proteins, such as bovine serum albumin (Adamczyk et al., 2012; Cheng et al., 2010), human plasma protein (Pinto et al., 2019), human serum albumin (Sekowski et al., 2014), and egg ovalbumin (Xie et al., 2017) have been previously reported. This property makes tannic acid useful for protein immobilization.

Although have been previously used in protein immobilization (Altun et al., 2015; Atacan & Özacar, 2015; Noma et al., 2020), to the best of author

knowledge, comprehensive adsorption study of protein on tannic acid modified Fe_3O_4 has never been done before. Bovine serum albumin (BSA) was used as a model protein in this study. Furthermore, the effect of adsorption pH, initial BSA concentration, and temperature was studied. From the obtained data, various isotherm adsorption and kinetic models, as well as the adsorption thermodynamics were investigated.

EXPERIMENTAL SECTION

Modification of Fe_3O_4 using tannic acid

The modification of Fe_3O_4 was done by following method used by (Atacan et al., 2017) with modification. Three grams of Fe_3O_4 (pure grade, Sigma Aldrich) was mixed with 60 mL of distilled water and dispersed by means of ultra-sonication for 15 min. A 1.5 g of tannic acid (pure grade, Sigma Aldrich) was dissolved into 40mL distilled water and was subsequently mixed with the iron mixture. The mixture was then mixed using an impeller at 200 rpm, 40°C for 2 h. The mixture was let cool down to room temperature before separation using an external magnet. The separated solid was then washed using ethanol (95%v/v) and demineralized water to remove unadsorbed tannic acid, and then dried using a vacuum oven at 70°C for 12 h. The modified iron oxide nanoparticle, denoted as Fe_3O_4-TA, was then stored in a closed lid bottle in a desiccator for further use and analysis.

Adsorption of BSA

The adsorption study of BSA was started by investigating the effect of solution's pH to adsorption, prior to kinetic and isotherm study. An 80 mg of Fe_3O_4 or Fe_3O_4-TA was dispersed into 5 mL of 1 mg/mL BSA (Merck) solution by means of ultra-sonication for 1 min. The solution's initial pH, varied from 3.6 to 5.6, was adjusted by using an acetate buffer. The mixture was then shaken using a shaker water bath at room temperature for 4 h. The BSA concentration before (Ci; mg/mL) and after adsorption (Cf; mg/mL) was then analyzed following Bradford method (Bradford, 1976). Adsorption capacity (qe; mg/mg) was calculated by following Equation **1**, where m is the mass of adsorbent (g) and V is the solution's volume (mL). The initial pH that gave the highest adsorption capacity was used in the kinetic and isotherm study. The kinetic study was done by following the previously described method, with initial BSA concentration of 1.5 mg/mL, initial temperature of 30 – 50°C, and sample was taken every 15 min until constant; while the isotherm study was done by varying initial BSA concentration from 0.5 to 1.5 mg/mL and initial temperature from 30 to 50°C.

$$qe = \frac{Ci - Cf}{m} \times V \qquad (1)$$

Characterization

The samples of Fe_3O_4 or Fe_3O_4-TA after BSA adsorption, denoted as Fe_3O_4-BSA or Fe_3O_4-TA-BSA, were analyzed to investigate the characteristics before and after protein adsorption. The samples obtained from initial BSA concentration 1.5 mg/mL and adsorption temperature 50°C were used for the characterization. The functional groups were characterized using Fourier Transform Infrared Spectroscopy (FTIR; Prestige 21 Shimadzu Instruments) by using KBr pellet method. The morphology was observed using Scanning Electron Microscope (SEM; HITACHI SU3500) and Transmission Electron Microscope (TEM; HITACHI HT7700). The sample crystallinity was analyzed using X-Ray Diffraction (XRD; BRUKER D8 Advance). Scherrer equation was employed to estimate the crystallite size (d in nm) from the obtained XRD spectra. The equation is presented in Equation **2**, where θ is the Bragg angle, K is Scherrer constant of 0.9, λ (0.15405 nm) is the wavelength of Cu K-α radiation, and β is the full width at half maximum (FWHM) peak.

$$d = \frac{K\,\lambda}{\beta\,cos\theta} \qquad (2)$$

RESULTS AND DISCUSSION

Characterization of iron oxide nanoparticles

Based on the FTIR spectra, presented in **Figure 1.a**, there are some notable peaks observed in the Fe_3O_4 samples, namely peaks at 3448.72 and 1604.77 cm^{-1} from O-H vibration of water molecules in the crystal structure and peak at 586.36 cm^{-1} of Fe-O vibration (Srivastava et al., 2011). After modification with tannic acid, the sample exhibited a sharper peak at 3448.72 cm^{-1} and a new peak at 1627.9 cm^{-1} due to the presence of O-H and C=O from tannic acid, respectively, with no change observed in the Fe-O peak. The tannic acid would be bonded to the surface of Fe_3O_4 via the phenolic hydroxyl functional groups (Bagtash et al., 2016). After protein adsorption, there were broad shoulder observed in both Fe_3O_4-BSA and Fe_3O_4-TA-BSA samples around 3000-3200 cm^{-1} due to overlap of O-H and N-H stretching, and new peak at 2924 cm^{-1} of C-H (Rahman et al., 2012; Ramzannezhad & Bahari, 2017). Both of these two peaks appeared stronger in the Fe_3O_4-TA-BSA sample on account of more protein being adsorbed on this sample.

The XRD spectra is presented in **Figure 1.b**. It could be observed that the Fe_3O_4 sample exhibited several peaks at 2θ and their respective hkl index as followed: 18.3° (111), 30.1° (202), 35.5° (311), 37.1° (222), 43.1° (400), 53.5° (422), 57° (511), and 62.6° (440) (Iida et al., 2007). All these peaks are commonly observed in Fe_3O_4 structure. Adsorption of BSA in both Fe_3O_4-BSA and Fe_3O_4-TA-BSA samples did not change the crystalline structure. Calculation of crystallite size was done by using Scherrer equation showed that Fe_3O_4-TA-BSA had the biggest diameter of 39.3 nm, compared to Fe_3O_4-BSA (38.4 nm) and Fe_3O_4 (35.8 nm). It is known that the Scherrer equation is a useful tool to estimate nanoparticle crystallite size

with high suitability to particle size measured using other methods, such as TEM visual observation (Londoño-Restrepo et al., 2019). The increase of particle size after protein adsorption has also been reported by previous researchers (Calatayud et al., 2014; Rahdar et al., 2019).

The morphology observation of Fe_3O_4, Fe_3O_4-BSA, and Fe_3O_4-TA-BSA was done by using SEM and TEM, as presented in **Figure 2**. From the SEM images (**Figure 2. a - c**), it could be seen that the adsorption of BSA did not give any changes to the morphology of Fe_3O_4. Similar observation of protein adsorption to the morphology of adsorbent has been reported before (Kristianto et al., 2020; Z. Liang et al., 2018). The presence of adsorbed protein on Fe_3O_4-TA was observed (**Figure 2.f**, white arrow), while none observed on Fe_3O_4-BSA (**Figure 2.e**). This finding might be due to low BSA adsorption on unmodified Fe_3O_4.

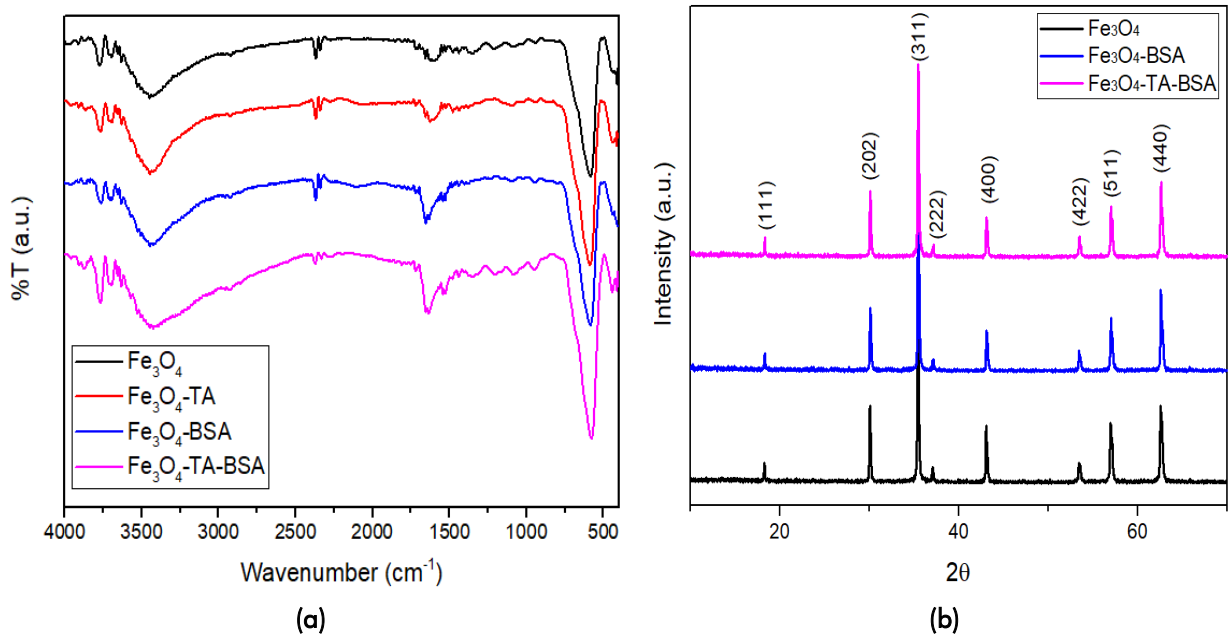

Figure 1. FTIR (a) and XRD (b) spectra of Fe_3O_4, Fe_3O_4-BSA and Fe_3O_4-TA-BSA

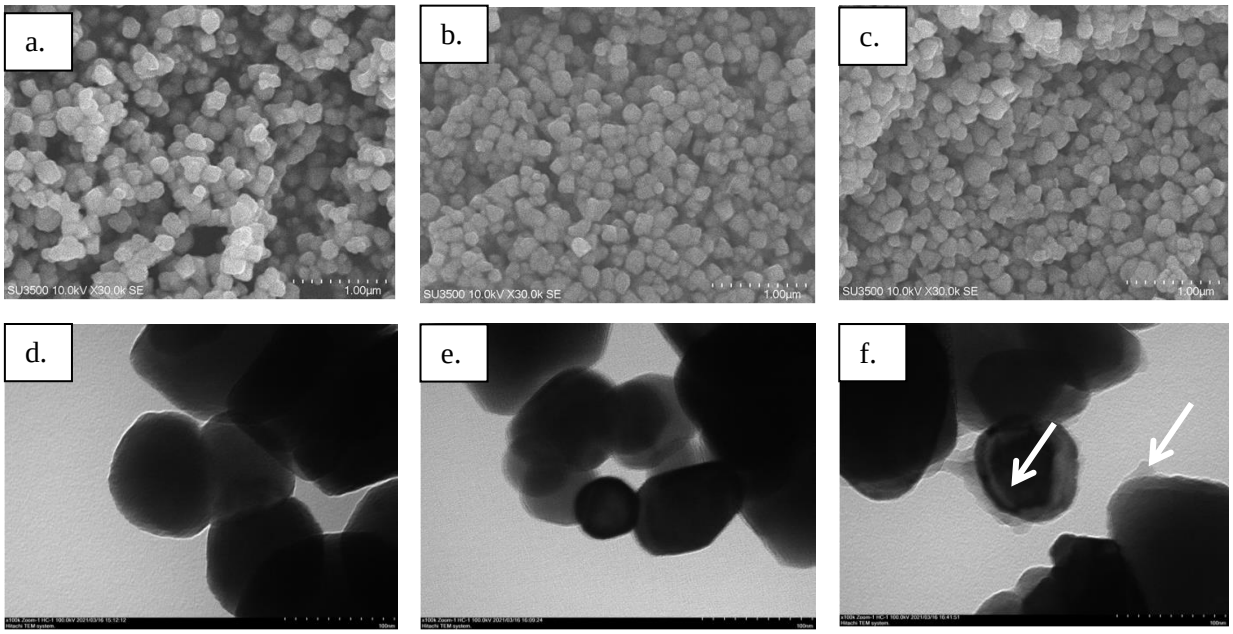

Figure 2. The SEM images and TEM images of Fe_3O_4 (a, d), Fe_3O_4-BSA (b, e), and Fe_3O_4-TA-BSA (c, f)

Effect of initial pH adsorption

The effect of initial pH to the BSA adsorption is presented in **Figure 3**. It could be observed that for both Fe_3O_4 and Fe_3O_4-TA, increase of pH from 3.6 to 4.8 gave increase to the qe, while further increase to 5.6 decreased the BSA adsorption. The highest BSA adsorption was observed at pH of 4.8, namely 12.61 mg/g for Fe_3O_4 and 31.34 mg/g for Fe_3O_4-TA. It is known that BSA possessed isoelectric point (pI) around 4.7-5.0 (Wiśniewska et al., 2015). This result is in accordance with previous researchers (Barreto et al., 2020; Y.-Y. Liang et al., 2007; Peng et al., 2004), where it was found that the best BSA adsorption was obtained at pH near pI. This was possible due to at its pI; BSA structure becomes more compact due to conformational shift of BSA structure (Barreto et al., 2020; Peng et al., 2004). This phenomenon resulted in minimum repulsion between BSA and adsorbent, resulting in maximum adsorption through dense packaging mechanism (Barreto et al., 2020). According to Fukuzaki et al. (1996), the adsorption phenomenon of protein is known to be controlled by the intrinsic properties of the protein more than the nature of the adsorbent. Furthermore, Barreto et al. (2020) found that the forces of BSA adsorption are beyond electrostatic interaction of BSA and adsorbent, but other forces, namely electrostatic and steric forces of protein-protein and protein-mineral and hydrophobic interaction on the hydrated surface are involved during BSA adsorption. Based on this result, pH 4.8 was further used for the kinetic and isotherm adsorption study.

Adsorption kinetics

The adsorption profile of BSA as a function of time is presented in **Figure 4.a**. It could be observed that a rapid BSA adsorption was observed at initial 75 min and relatively constant until 210 min. Based on the experimental data, several kinetic models were used to investigate the adsorption mechanism. The models used and their linearized forms are presented in **Table 1**, and the fitting results for these models are shown in **Table 2**. It could be seen from the R^2 and χ^2 value, the pseudo 1st order kinetic model was poorly fitted to the experimental data, and while pseudo 2nd order kinetic model was the most suitable to describe the adsorption kinetic of BSA on both Fe_3O_4 and Fe_3O_4-TA. The Elovich kinetic model was moderately suitable with R^2 values ranging from 0.78 to 0.94, and relatively low χ^2. Both of the data from this model are relatively well fitted to the experimental data, as shown in **Figure 4.b**. The suitability of pseudo 2nd order and Elovich kinetics suggested that the BSA adsorption in this study was chemisorption. This was plausible due to electrostatic interaction in Fe_3O_4-BSA and electrostatic – hydrophobic interaction in Fe_3O_4-TA-BSA. As for the intraparticle diffusion model, a 2-phase adsorption plot was observed (figure not shown), which usually indicates a 2 rate determining steps of surface adsorption and intraparticle diffusion. Albeit the high R^2 value of intraparticle diffusion model, this model was relatively not suitable for describing the adsorption in this study, where the data obtained from the model was deviated from the equilibrium, as shown in **Figure 4.b**.

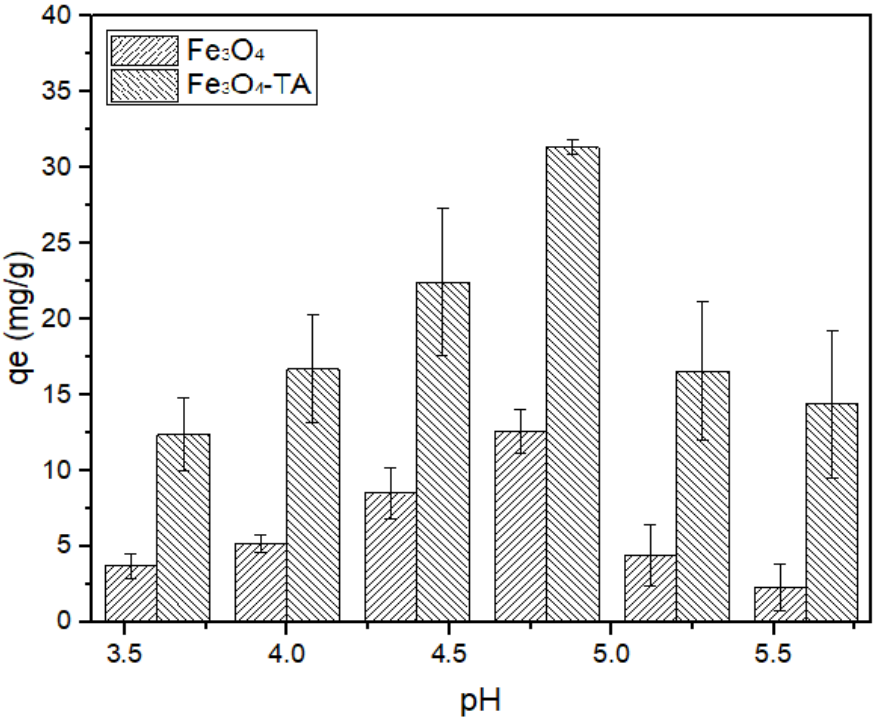

Figure 3. The effect of initial pH to BSA adsorption

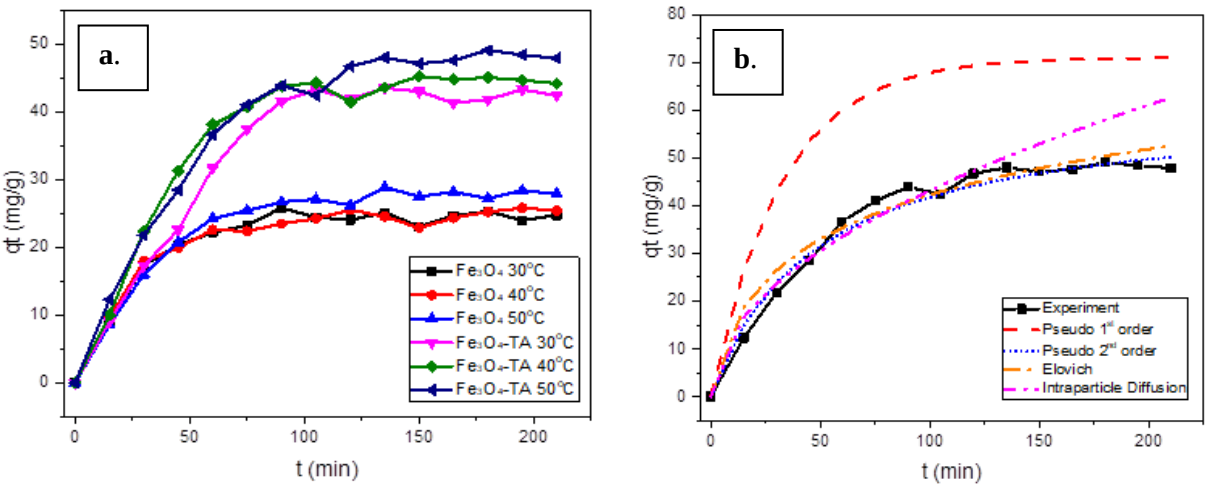

Figure 4. BSA adsorption capacity versus time (**a**) and suitability of model and experimental data (Fe_3O_4-TA-BSA, 1.5 mg/mL, 50°C) (**b**)

Table 1. Kinetic models used in this study

Model	Linearized equation	Reference
Pseudo 1st order	$\ln(qe - qt) = \ln(qe) - k_1 t$	(Azizian, 2004)
Pseudo 2nd order	$\frac{t}{qt} = \frac{t}{qe} + \frac{1}{k_2 qe^2}$	(Azizian, 2004)
Elovich	$qt = \frac{1}{\beta}\ln(\alpha\beta) + \frac{1}{\beta}\ln(t)$	(Riahi et al., 2017)
Intraparticle diffusion	$qt = k_d t^{\frac{1}{2}}$	(Riahi et al., 2017)

Table 2. Kinetic parameters of BSA adsorption

		Fe_3O_4			Fe_3O_4-TA		
Model	Parameters	30°C	40°C	50°C	30°C	40°C	50°C
Pseudo 1st order	k_1 (min^{-1})	0.0195	0.0186	0.0224	0.0263	0.0329	0.0312
	qe (mg/g)	9.62	13.03	16.83	38.74	45.18	70.99
	R^2	0.6119	0.7805	0.8423	0.792	0.7421	0.9625
	χ^2	136.106	94.365	64.972	8.998	8.082	190.251
Pseudo 2nd order	k_2 (g/mg.min)	0.0023	0.0019	0.0012	0.0003	0.0005	0.0003
	qe (mg/g)	26.95	27.70	32.36	57.14	54.94	61.34
	R^2	0.987	0.9918	0.9875	0.9429	0.9656	0.9833
	χ^2	2.905	1.211	1.854	5.148	5.508	1.9365
Elovich	α (1/mg.min)	4.2706	4.4408	2.5409	2.0264	2.9274	2.5707
	β (g/mg)	0.1937	0.1946	0.1426	0.0725	0.0790	0.0695
	R^2	0.7812	0.855	0.8872	0.8941	0.8786	0.9496
	χ^2	4.2308	2.5176	3.7587	11.8991	11.3896	6.1765
Intraparticle diffusion	k_d ($mg/g.t^{1/2}$)	2.8024	2.5703	2.8524	4.0193	4.4937	4.3197
	R^2	0.9744	0.9258	0.97222	0.9385	0.9586	0.9729
	χ^2	42.3599	22.3866	23.1263	24.5844	37.7500	13.8832

Effect of initial BSA concentration and temperature

Adsorption at various initial concentrations and adsorption temperatures could affect the adsorption performance of BSA. It could be observed in **Figure 5** that increase of BSA initial concentration and temperature could increase the equilibrium adsorption capacity for both Fe_3O_4 and Fe_3O_4-TA. The increase of initial BSA concentration could increase interaction between adsorbate and adsorbent, resulting in more protein adsorbed (Rahdar et al., 2019). Similar trend was also observed in previous studies (Kim et al., 2020; Mahdavinia & Etemadi, 2019; Rahdar et al., 2019). The effect of temperature on adsorption capacity showed that BSA adsorption on Fe_3O_4 and Fe_3O_4-TA was an endothermic process, as the adsorption capacity increased with the increase of temperature.

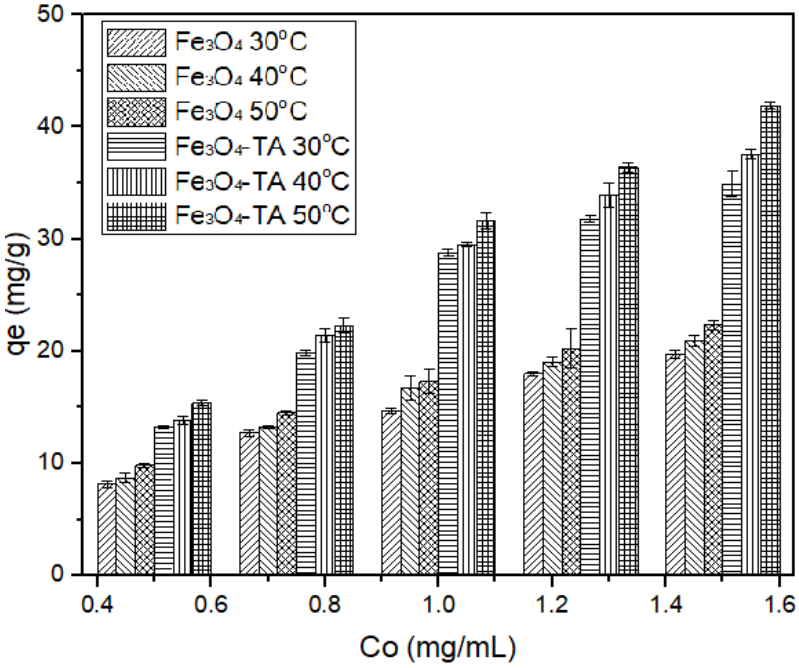

Figure 5. Effect of initial BSA concentration and temperature to equilibrium adsorption capacity

Isotherm adsorption

The adsorption data of BSA on Fe_3O_4 and Fe_3O_4-TA at various initial BSA concentration and temperature were investigated using several isotherm adsorption models, namely Langmuir, Freundlich, Temkin, and Dubinin Raduskevich (DR), presented in **Table 3**. The fitting of experimental data was done using linear regression of the isotherm models; the parameters obtained are presented in **Table 4**.

The Langmuir isotherm model assumes monolayer adsorption on homogeneous surfaces with similar adsorption energy. The qm (mg/g), maximum adsorption capacity, showed that BSA adsorption on Fe_3O_4-TA increase five-folds. This was possible due to the complex formation between tannic acid and BSA through tannic acid bound in BSA's ligand binding sites in hydrophobic cavities (Xie et al., 2017). The Langmuir separation factor, R_L, lies between 0 to 1, indicating a favorable adsorption process (Al-Ghouti & Da'ana, 2020). Comparison of BSA adsorption using various adsorbent reported in the literature presented in **Table 5**. It could be seen that the Fe_3O_4-TA gave comparable, if not higher, BSA maximum monolayer adsorption capacity compared to other adsorbents.

Freundlich isotherm model describes multilayer adsorption on heterogeneous surfaces with nonuniform adsorption energy. The Freundlich constant, Kf (L/mg), indicates adsorption capacities, showed two times higher value for Fe_3O_4-TA compared to Fe_3O_4. The 1/n value describes the intensity of adsorption. For this experiment all 1/n values ranged from 0 to 1, indicating favorable adsorption. Temkin isotherm assumes adsorption heat as a function of temperature and linearly decreases adsorbate molecules due to increase of adsorbate surface coverage (Al-Ghouti & Da'ana, 2020). The α value of Temkin isotherm indicates maximum binding energy. With the increase of temperature, the α values also increased, implying that the BSA adsorption was endothermic (Aljeboree et al., 2017). DR isotherm adsorption model is used on assumption of Gaussian distributed energy of adsorption onto heterogeneous surfaces (Al-Ghouti & Da'ana, 2020), which is shown by the Polanyi potential (ε). The ε is calculated from equilibrium concentration (Ce; mg/L); R is the gas constant (J/mol.K); and T is absolute temperature (K). From the adsorption model, it could be observed that the DR maximum adsorption capacity (qs; mg/L) of Fe_3O_4-TA increased twofold, compared to Fe_3O_4. This result is consistent with the Freundlich isotherm adsorption.

Based on the R^2 value, it could be seen that Langmuir, Freundlich, and Temkin isotherm exhibited high $R^2 > 0.95$, while DR isotherm exhibited lower R^2. Further determination of suitability of the isotherm model to the experimental data was done by calculating the χ^2 value, presented in equation **3**, and the experimental data vs model fitting presented in **Figure 6**. From the χ^2 value, the Freundlich isotherm model gave the lowest χ^2 value than other models. Furthermore, according to Latour (2015) the Langmuir isotherm adsorption model might not be suitable to perfectly describe the protein adsorption, due to the tendency of protein to aggregate thus forming a multilayer adsorption. Thus, the Freundlich isotherm adsorption model is the most suitable to describe the experimental data obtained and this model was further used to estimate the thermodynamic parameters.

$$\chi^2 = \sum_{i=1}^{n} \frac{(qe\ model - qe\ data)^2}{qe\ data} \qquad (3)$$

Table 3. Isotherm models used in this study (Al-Ghouti & Da'ana, 2020; Kristianto et al., 2019)

Isotherm	Equation	Linearized equation
Langmuir	$qe = \frac{K_L.qm.Ce}{1+K_L.Ce}$ $R_L = \frac{1}{1+K_L Ci}$	$\frac{Ce}{qe} = \frac{Ce}{qm} + \frac{1}{K_L.qm}$
Freundlich	$qe = Kf.Ce^{\frac{1}{n}}$	$\log(qe) = \log(Kf) + \frac{1}{n}.\log(Ce)$
Temkin	$qe = \beta.\ln(\alpha.Ce)$	$qe = \beta.\ln(\alpha) + \beta.\ln(Ce)$
Dubinin Raduskevich	$qe = qs.e^{-K\varepsilon^2}$ $\varepsilon = RT.\ln(1+\frac{1}{Ce})^2$	$\ln(qe) = qs - K\varepsilon^2$

Table 4. Parameters of isotherm adsorption isotherm models

Isotherm Model	Parameters	Fe_3O_4			Fe_3O_4-TA		
		30°C	40°C	50°C	30°C	40°C	50°C
Langmuir	K_L (L/mg)	0.6456	0.7817	0.8960	0.2356	0.2524	0.3041
	qm (mg/g)	46.51	45.05	44.64	222.22	234.23	222.22
	R_L	0.522-0.771	0.476-0.742	0.440-0.704	0.748-0.897	0.734-0.893	0.697-0.871
	R^2	0.9862	0.9967	0.9913	0.9885	0.9929	0.9878
	χ^2	0.1813	0.0391	0.1183	0.4843	0.3964	0.2301
Freundlich	Kf (L/mg)	18.45	20.12	21.54	42.29	47.48	54.87
	1/n	0.7255	0.7056	0.6749	0.8617	0.869	0.9032
	R^2	0.9781	0.9989	0.9895	0.9723	0.9797	0.9885
	χ^2	0.1634	0.0098	0.0826	0.5064	0.4400	0.2044
Temkin	α (L/mg)	6.958	7.618	8.035	7.185	7.585	7.425
	β (J/mol)	9.390	9.721	10.14	19.38	20.67	23.59
	R^2	0.9560	0.9821	0.9689	0.9827	0.9845	0.9677
	χ^2	0.2431	0.1220	0.1788	0.2331	0.2455	0.6923
Dubinin-Raduskevich (DR)	K (mol^2/J^2)	0.0157	0.012	0.0118	0.0123	0.0098	0.0089
	qs (mg/g)	19.02	20.06	21.41	36.16	37.90	40.64
	R^2	0.9138	0.9126	0.9079	0.9471	0.9363	0.8875
	χ^2	0.6693	0.7039	0.7000	0.8073	1.12	2.164

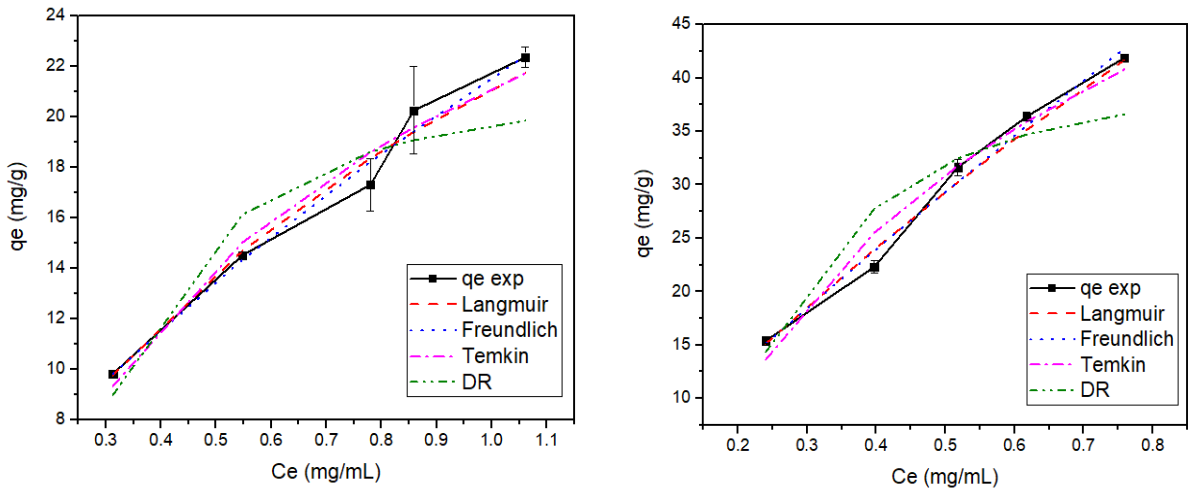

Figure 6. Fitting of experimental data and model of BSA adsorption on Fe_3O_4 (a) and Fe_3O_4-TA at 50°C

Table 5. Comparison of BSA adsorption using various adsorbent

Adsorbent	Maximum monolayer adsorption capacity (mg/g)	Reference
Fe_3O_4-TA	222.22	This study
$ZnFe_2O_4$	250.04	(R. Liu et al., 2017)
Silica coated $MnFe_2O_4$	164	(H. F. Liang & Wang, 2010)
κ-carrageenan/ carboxymethyl chitosan modified iron oxide nanoparticles	73.3	(Mahdavinia & Etemadi, 2019)
$Fe_3O_4/C/MnO_2$	129.9	(Kim et al., 2020)
Gold nanoparticles	109.54	(Maleki et al., 2017)
Fe_3O_4/SiO_2/mesoporous SiO_2	289	(Hou et al., 2015)
Chitosan coated Fe_3O_4	96.5	(Shen et al., 2014)
carboxymethyl chitosan modified iron oxide nanoparticles	159.51	(Wang et al., 2015)

Table 6. Thermodynamic parameters form BSA adsorption on Fe_3O_4 and Fe_3O_4-TA

Temperature (K)	Fe_3O_4			Fe_3O_4-TA		
	ΔG° (kJ/mol)	ΔH° (kJ/ mol)	ΔS° (kJ/mol K)	ΔG° (kJ/mol)	ΔH° (kJ/ mol)	ΔS° (J/mol K)
303	-62.84	6.31	0.23	-64.93	10.58	0.25
313	-65.13			-67.37		
323	-67.40			-69.91		

Thermodynamic of BSA adsorption

Thermodynamic parameters of BSA adsorption on Fe_3O_4 and Fe_3O_4-TA, namely Gibbs free energy (ΔG°), enthalpy (ΔH°) and entropy (ΔS°), were estimated from the equilibrium isotherm adsorption to study the nature of BSA adsorption. Estimation was done by using van't Hoff equation **4**, where R is gas constant (8.314 J/mol.K), T is the absolute temperature (K), and K° is the equilibrium constant (Chen et al., 2021). At equilibrium, ΔG=0 resulting in equation **5**. Combining equation **5** with the 3rd principles of thermodynamics (equation **6**), equation **7** is obtained.

$$\Delta G = \Delta G° + R.T.\ln(K°) \quad (4)$$

$$\Delta G° = -R.T.\ln(K°) \quad (5)$$

$$\Delta G° = \Delta H° - T.\Delta S° \quad (6)$$

$$\ln(K°) = \frac{-\Delta H°}{R}.\frac{1}{T} + \frac{\Delta S°}{R} \quad (7)$$

The K° value in Equation **7** should be dimensionless thus conversion of Kf should be done prior to thermodynamic parameters calculation, as shown in equation **8** (Lima et al., 2019; Zhou & Zhou, 2014).

$$K° = Kf\left(\frac{L}{mg}\right).1000\frac{mg}{g}.55.51\frac{mol}{L}.Mr\ BSA\left(\frac{g}{mol}\right) \quad (8)$$

The calculated thermodynamic parameters are presented in **Table 6**. For both adsorbents, negative ΔG° was obtained for all temperatures, indicating spontaneous adsorption process. Furthermore form the magnitude of ΔG°, it could be inferred whether the adsorption is physisorption (0 to -20 kJ/mol) or chemisorption (-80 to -400 kJ/mol) (Q.-S. Liu et al., 2010). Based on the obtained ΔG° values, it could be said that the BSA adsorption was mainly physical adsorption enhanced by chemisorption (Q.-S. Liu et al., 2010; Yu et al., 2004). The adsorption enthalpies were positive for both adsorbent, indicating endothermic nature of the adsorption. Furthermore, the positive value of ΔS° suggests the randomness and spontaneity of BSA adsorption.

CONCLUSIONS

In this study, the effect of tannic acid modification on Fe_3O_4 to the BSA adsorption was reported. Successful modification of Fe_3O_4 was confirmed using FTIR analysis. Furthermore, it was found that Fe_3O_4 modified with tannic acid (Fe_3O_4-TA) could improve the adsorption of BSA, compared to unmodified one. The modification and BSA adsorption did not change the Fe_3O_4 morphology as well as crystalline structure. However, a bigger crystalline diameter was observed after protein adsorption. At various pHs, it was found that pH 4.8 was the best pH for both Fe_3O_4 and Fe_3O_4-TA. Investigation of kinetic adsorption showed that the adsorption was following pseudo 2nd kinetic order and constant after 210 min. Variations of initial BSA concentration and adsorption temperature were used to study the isotherm adsorption of BSA. It was found that the Langmuir monolayer adsorption capacity increased five times for adsorbent Fe_3O_4-TA compared to Fe_3O_4. The superior performance of Fe_3O_4-TA was possible due to complex formation of BSA and tannic acid. Freundlich model was found to be the most suitable isotherm adsorption model and its constant was used in the thermodynamic

calculation. Analysis of the calculated thermodynamic parameters suggested that the BSA adsorption was spontaneous with increase of randomness ($\Delta G°<0$; $\Delta S°>0$). The BSA adsorption on both adsorbents was also endothermic, as also shown in the increase of equilibrium adsorption capacity with the increase of adsorption temperature. The results obtained in this study suggest that modification of Fe_3O_4 could be a simple but effective approach in increasing protein adsorption.

ACKNOWLEDGEMENTS

This work was funded by Parahyangan Catholic University Centre of Research and Community Service with Contract No. III/LPPM/2021-02/33-P. The authors are grateful for the funding provided.

REFERENCES

Adamczyk, B., Salminen, J.-P., Smolander, A., & Kitunen, V. (2012). Precipitation of proteins by tannins: effects of concentration, protein/tannin ratio and pH. *Int J Food Sci Technol, 47*(4), 875-878.

Al-Ghouti, M. A., & Da'ana, D. A. (2020). Guidelines for the use and interpretation of adsorption isotherm models: A review. *J Hazard Mater, 393*, 122383.

Aljeboree, A. M., Alshirifi, A. N., & Alkaim, A. F. (2017). Kinetics and equilibrium study for the adsorption of textile dyes on coconut shell activated carbon. *Arab J Chem, 10*, S3381-S3393.

Altun, S., Çakıroğlu, B., Özacar, M., & Özacar, M. (2015). A facile and effective immobilization of glucose oxidase on tannic acid modified CoFe2O4 magnetic nanoparticles. *Colloids Surf B, 136*, 963-970.

Atacan, K., Cakiroglu, B., & Ozacar, M. (2017). Efficient Protein Digestion Using Immobilized Trypsin onto Tannin Modified Fe_3O_4 Magnetic Nanoparticles. *Colloids Surf B, 156*, 9-18.

Atacan, K., Güy, N., Çakar, S., & Özacar, M. (2019). Efficiency of glucose oxidase immobilized on tannin modified $NiFe_2O_4$ nanoparticles on decolorization of dye in the Fenton and photo-biocatalytic processes. *J Photochem Photobiol A, 382*, 111935.

Atacan, K., & Özacar, M. (2015). Characterization and immobilization of trypsin on tannic acid modified Fe3O4 nanoparticles. *Colloids Surf B, 128*, 227–236.

Azizian, S. (2004). Kinetic models of sorption: a theoretical analysis. *J Colloid Interface Sci 276*, 47–52.

Bagtash, M., Yamini, Y., Tahmasebi, E., Zolgharnein, J., & Dalirnasab, Z. (2016). Magnetite nanoparticles coated with tannic acid as a viablesorbent for solid-phase extraction of Cd^{2+},$Co^{2+}$and Cr^{3+}. *Microchimica Acta, 183*, 449-456.

Barreto, M. S. C., Elzinga, E. J., & Alleoni, L. R. F. (2020). The molecular insights into protein adsorption on hematite surface disclosed by in-situ ATR-FTIR/2D-COS study. *Sci Rep, 10*(13441).

Bele, A. A., jadhav, V. M., & Kadam, V. J. (2010). Potential of Tannins: A Review. *Asian Journal of Plant Sciences, 9*(4), 209-214.

Bradford, M. M. (1976). A Rapid and Sensitive Method for the Quantitation of Microgram Quantities of Protein Utilizing the Principle of Protein-Dye Binding. *Anal Biochem, 72*, 248-254.

Cagliani, R., Gatto, F., & Bardi, G. (2019). Protein Adsorption: A Feasible Method for Nanoparticle Functionalization? *Materials, 12*(12), 1991.

Calatayud, M. P., Sanz, B., Raffa, V., Riggio, C., Ibarra, M. R., & Goya, G. F. (2014). The effect of surface charge of functionalized Fe3O4 nanoparticles on protein adsorption and cell uptake. *Biomaterials, 35*(24), 6389-6399.

Cao, M., Li, Z., Wang, J., Ge, W., Yue, T., Li, R., Colvin, V. L., & Yu, W. W. (2012). Food related applications of magnetic iron oxide nanoparticles: Enzyme immobilization, protein purification, and food analysis *Trends Food SciTechnol, 27*, 47-56.

Chen, T., Da, T., & Ma, Y. (2021). Reasonable calculation of the thermodynamic parameters from adsorption equilibrium constant. *J Mol Liq, 322*, 114980.

Cheng, T.-J., Hsiao, H.-Y., Chung, C.-Y., Chen, P.-C., & Chen, R. L. C. (2010). Determination of tannic acid after precipitation with bovine serum albumin by visible light scattering in a flow injection system. *Microchimica Acta, 169*, 117-122.

Cobellis, G., Trabalza-Marinucci, M., & Yu, Z. (2016). Critical evaluation of essential oils as rumen modifiers in ruminant nutrition: A review. *Sci Total Environ, 545-546*, 556-568.

Dalvand, A., Nabizadeh, R., Ganjali, M. R., Khoobi, M., Nazmara, S., & Mahvi, A. H. (2016). Modeling of Reactive Blue 19 azo dye removal from colored textile wastewater using L-arginine-functionalized Fe_3O_4 nanoparticles: Optimization, reusability, kinetic and equilibrium studies. *J Magn Magn Mater, 404*, 179-189.

Dorniani, D., Hussein, M. Z., Kura, A. U., Fakurazi, S., Shaari, A. H., & Ahmad, Z. (2012). Preparation of Fe_3O_4 magnetic nanoparticles coated with gallic acid for drug delivery. *Int J Nanomedicine, 7*, 5745-5756.

Fukuzaki, S., Urano, H., & Nagata, K. (1996). Adsorption of bovine serum albumin onto metal oxide surfaces. *J Ferment Bioeng, 81*, 163–167

Hou, X., Xu, H., Pan, L., Tian, Y., Zhang, X., Ma, L., Li, Y., & Zhao, J. (2015). Adsorption of bovine serum albumin on superparamagnetic composite microspheres with a Fe_3O_4/SiO_2 core and mesoporous SiO_2 shell. *RSC Adv, 5*(126), 103760-103766.

Iida, H., Takayanagi, K., Nakanishi, T., & Osaka, T. (2007). Synthesis of Fe_3O_4 nanoparticles with various sizes and magnetic properties by controlled hydrolysis. *J Colloid Interf Sci, 314*, 274–280.

Kim, C.-H., Zhang, Z.-F., Wang, L.-S., & Sun, T. (2020). Preparation of MnO_2-impregnated carbon-coated Fe_3O_4 nanocomposites and their application for bovine serum albumin adsorption. *Rare Met, 39*(3), 1151–1158.

Kristianto, H., Daulay, N., & Arie, A. A. (2019). Adsorption of Ni(II) Ion onto Calcined Eggshells: A Study of Equilibrium Adsorption Isotherm. *Indones J Chem, 19*(1), 143 - 150.

Kristianto, H., Reynaldi, E., Prasetyo, S., & Sugih, A. K. (2020). Adsorbed Leucaena protein on citrate modified Fe_3O_4 nanoparticles: synthesis, characterization, and its application as magnetic coagulant. *Sustain Environ Res, 30*, 32.

Latour, R. A. (2015). The Langmuir isotherm: A commonly applied but misleading approach for the analysis of protein adsorption behavior. *J Biomed Mater Res Part A, 103*(3), 949-958.

Laurent, S., Forge, D., Port, M., Roch, A., Robic, C., Elst, L. V., & Muller, R. N. (2008). Magnetic Iron Oxide Nanoparticles: Synthesis, Stabilization, Vectorization, Physicochemical Characterizations, and Biological Applications. *Chem Rev, 108*, 2064–2110.

Lesiak, B., Rangam, N., Jiricek, P., Gordeev, I., Tóth, J., Kövér, L., Mohai, M., & Borowicz, P. (2019). Surface Study of Fe_3O_4 Nanoparticles Functionalized With Biocompatible Adsorbed Molecules. *Front Chem, 7*, 642.

Liang, H. F., & Wang, Z. C. (2010). Adsorption of bovine serum albumin on functionalized silica-coated magnetic $MnFe_2O_4$ nanoparticles. *Mater Chem Phys, 124*, 964–969.

Liang, Y.-Y., Zhang, L.-M., Li, W., & Chen, R.-F. (2007). Polysaccharide-modified iron oxide nanoparticles as an effective magnetic affinity adsorbent for bovine serum albumin. *Colloid Polym Sci, 285*, 1193–1199.

Liang, Z., Yang, Z., Yuan, H., Wang, C., Qi, J., Liu, K., Cao, R., & Zheng, H. (2018). A Protein@Metal−Organic Framework Nanocomposite for pH-Triggered Anticancer Drug Delivery. *Dalton Trans, 47*(30), 10223-10228.

Lima, E. C., Hosseini-Bandegharaei, A., Moreno-Pirajá, J. C., & Anastopoulos, I. (2019). A critical review of the estimation of the thermodynamic parameters on adsorption equilibria. Wrong use of equilibrium constant in the Van't Hoof equation for calculation of thermodynamic parameters of adsorption. *J Mol Liq, 273*, 425-434.

Liu, Q.-S., Zheng, T., Wang, P., Jiang, J.-P., & Li, N. (2010). Adsorption isotherm, kinetic and mechanism studies of some substituted phenols on activated carbon fibers. *Chem Eng J, 157*(2-3), 348-356.

Liu, R., Cheng, Y., Li, Y., Zhang, Q., Jia, B., Wang, D., & Fan, R. (2017). Adsorption Kinetics and Adsorption Isotherms of Bovin Serum Albumin (BSA) onto Magnetic $ZnFe_2O_4$ Nanoparticles. *J Nanosci Nanotechnol, 17*, 2899-2905.

Londoño-Restrepo, S. M., Jeronimo-Cruz, R., Millán-Malo, B. M., Rivera-Muñoz, E. M., & Rodriguez-García, M. E. (2019). Effect of the Nano Crystal Size on the X-ray Diffraction Patterns of Biogenic Hydroxyapatite from Human, Bovine, and Porcine Bones. *Scientific Reports, 9*(5915).

Mahdavinia, G. R., & Etemadi, H. (2019). Surface modification of iron oxide nanoparticles with k-carrageenan/ carboxymethyl chitosan for effective adsorption of bovine serum albumin. *Arab J Chem, 12*(8), 3692-3703.

Maleki, M. S., Moradi, O., & Tahmasebi, S. (2017). Adsorption of albumin by gold nanoparticles: Equilibrium and thermodynamics studies. *Arab J Chem, 10*, S491-S502.

Neha, R., Jaiswal, A., Bellare, J., & Sahu, N. K. (2017). Synthesis of Surface Grafted Mesoporous Magnetic Nanoparticles for Cancer Therapy. *J Nanosci Nanotechnol, 17*, 5181–5188.

Noma, S. A. A., Ulu, A., Acet, Ö., Sanz, R., Sanz-Pérez, E. S., Odabaşı, M., & Ateş, B. (2020). Comparative study of ASNase Immobilization on Tannic Acid-Modified Magnetic Fe_3O_4/SBA-15 Nanoparticles to Enhance Stability and Reusability. *New J Chem, 44*, 4440-4451.

Peng, Z. G., Hidajat, K., & Uddin, M. S. (2004). Adsorption of bovine serum albumin on nanosized magnetic particles. *J Colloid Interface Sci, 271*(2), 277–283.

Pinto, A. F., Nascimento, J. M., Sobral, R. V. S., Amorim, E. L. C. d., Silva, R. O., & Leite, A. C. L. (2019). Tannic acid as a precipitating agent of human plasma proteins. *Eur J Pharm Sci, 138*, 105018.

Rahdar, S., Rahdar, A., Ahmadi, S., & Trant, J. F. (2019). Adsorption of bovine serum albumin (BSA) by bare magnetite nanoparticles with surface oxidative impurities that prevent aggregation. *Can J Chem, 97*(577-583).

Rahman, Z. U., Dong, Y., Ren, C., Zhang, Z., & Chen, X. (2012). Protein Adsorption on Citrate Modified Magnetic Nanoparticles. *J Nanosci Nanotechnol 12*, 2598–2606.

Ramzannezhad, A., & Bahari, A. (2017). Characteristics of Fe_3O_4, α -Fe_2O_3, and γ -Fe_2O_3 Nanoparticles as Suitable Candidates in the Field of Nanomedicine. *J Supercond Nov Magn, 30*(8), 2165-2174.

Riahi, K., Chaabane, S., & Thayer, B. B. (2017). A kinetic modeling study of phosphate adsorption onto Phoenix dactylifera L. date palm fibers in batch mode. *J Saudi Chem Soc, 21*, S143–S152.

Sekowski, S., Ionov, M., Kaszuba, M., Mavlyanov, S., Bryszewska, M., & Zamaraeva, M. (2014). Biophysical studies of interaction between hydrolysable tannins isolated from Oenothera gigas and Geranium sanguineum with human serum albumin. *Biointerfaces, 123*, 623-628.

Shen, M., Yu, Y., Fan, G., Chen, G., Jin, Y. M., Tang, W., & Jia, W. (2014). The synthesis and characterization of monodispersed chitosan-coated Fe_3O_4 nanoparticles via a facile one-step solvothermal process for adsorption of bovine serum albumin. *Nanoscale Res Lett, 9*, 296.

Srivastava, V., Singh, P. K., Weng, C. H., & Sharma, Y. C. (2011). Economically viable synthesis of Fe_3O_4 nanoparticles and their characterization. *Pol J Chem Technol, 13*(2), 1-5.

Wang, Z., Cai, R., Yue, T., Yuan, Y., & Niu, C. (2015). Preparation and Characterization of Carboxymethyl Chitosan Modified Magnetic Nanoparticles for Bovine Serum Albumin Adsorption. *Sep Sci Technol, 50*(2), 299-309.

Wiśniewska, M., Szewczuk-Karpisz, K., & Sternik, D. (2015). Adsorption and thermal properties of the bovine serum albumin–silicon dioxide system. *J Therm Anal Calorim, 120*, 1355–1364.

Wu, W., He, Q., & Jiang, C. (2008). Magnetic Iron Oxide Nanoparticles: Synthesis and Surface Functionalization Strategies. *Nanoscale Res Lett, 3*, 397–415.

Xie, L., Wehling, R. L., Ciftci, O., & Zhang, Y. (2017). Formation of complexes between tannic acid with bovine serum albumin, egg ovalbumin and bovine beta-lactoglobulin. *Food Res Int, 102*, 195-202.

Xu, J.-K., Zhang, F.-F., Sun, J.-J., Sheng, J., Wang, F., & Sun, M. (2014). Bio and Nanomaterials Based on Fe_3O_4. *Molecules, 19*, 21506-21528.

Yu, Y., Zhuang, Y.-Y., Wang, Z.-H., & Qiu, M.-Q. (2004). Adsorption of water-soluble dyes onto modified resin. *Chemosphere, 54*(3), 425-430.

Zhou, X., & Zhou, X. (2014). The unit problem in the thermodynamic calculation of adsorption using the Langmuir equation. *Chem Eng Commun, 201*(11), 1459-1467.